Thin Films of $(Fe_{1-x}Co_x)_3P$ and $Fe_3(P_{1-x}Te_x)$ from the Co-Decomposition of Organometallic Precursors by MOCVD

*Andrew P. Leitner, Jing-Han Chen, Desmond E. Schipper, Kenton H. Whitmire**

Department of Chemistry MS60, Rice University, 6100 Main Street, Houston, TX, 77005, USA

Contact information for the corresponding author:

Email: whitmir@rice.edu

Phone: 713-348-5650

Abstract

A new method for preparing thin films of ternary transition metal phosphides has been developed. The ferromagnetic compound Fe_3P has been doped with cobalt and tellurium by decomposing $H_2Fe_3(CO)_9P^tBu$ with $Co_3(CO)_9P^tBu$, or $H_2Fe_3(CO)_9Te$ via Metal-Organic Chemical Vapor Deposition (MOCVD) onto a quartz substrate. Solid mixtures of the organometallic clusters were vaporized and decomposed at 350 ºC to produce films that were subsequently annealed under vacuum at 650 ºC for 24 hours to afford crystalline films of $(Fe_{1-x}Co_x)_3P$ ($0.09<x<0.22$) and $Fe_3(P_{1-x}Te_x)$ ($0.04<x<0.42$). The films exhibit phase purity as confirmed by powder X-ray diffraction and X-ray photoelectron spectroscopy, which also confirmed the homogeneity of the films. Increasing the amount of doped elements were tracked by changes in the unit cell constants and elemental ratios by ICP-OES analysis. Field-dependent magnetization measurements showed magnetic hysteresis with similar magnetic saturation values for each doped material. Thermogravimetric analysis was used to compare the Curie temperatures (T_c) of pristine Fe_3P (thin film) and the doped films; Co-doping was found to lower the T_c by up to 7 °C and Te-doping had no observable effect on the T_c.

Introduction

Research in transition-metal phosphide materials has burgeoned in recent years with reports of robust catalytic activity,[1–8] magnetic properties,[9–11] and energy storage capacity.[12–14] The similarity of their binary solid crystal structures gives the flexibility of designing materials by introducing a third element.[15–17] The magnetic properties of the system $(Fe_{1-x}M_x)_3P$ have previously been manipulated by varying the dopant M (M = Mn, Co, Cr, and Ni) by conventional solid state synthesis.[11,18–20] However, the formation of these compounds in a single, pure phase remains challenging.

In recent years, our group has developed a clean route to such compounds as phase-pure materials through the use of molecular precursors. Phase pure Fe_2P and $Fe_{2-x}Mn_xP$ nanorods were grown by solution-based decomposition of single-source organometallic precursors.[21,22] In the case of $Fe_{2-x}Mn_xP$ nanorods, the desired elemental composition was determined by that of the molecular precursor, $FeMn(CO)_8(\mu\text{-}PH_2)$. Others have found $Fe(CO)_4PH_3$ and $[(CO)_4Cr(\mu\text{-}PH_2)]_2$ decompose in surfactant media to yield single phases of FeP and CrP respectively.[23,24] In addition to nanoparticle synthesis, similar organometallic compounds were used to synthesize phase pure thin films of Fe_3P by Metal-Organic Chemical Vapor Deposition (MOCVD).[25] The synthesis of metal-phosphides under vacuum by MOCVD allows for more mild reaction conditions and the ability to deposit thin films on any substrate.

An alternative route to ternary phases is to co-decompose multiple organometallic precursors that possess similar geometries, solubilities and/or volatilities, which allows for a much wider range of achievable compositions. Jin et al. combined $Fe(CO)_4(SiCl_3)_2$ and $Co(CO)_4SiCl_3$ to form a homogenous liquid, which was used as an MOCVD feedstock to produce $Fe_{1-x}Co_xSi$ nanowires.[26,27] Doping can have large impacts on the properties of the metal pnictides.[28,29] Previous studies show that the Curie temperature of the Fe_3P system can be reduced by up to 500 K by replacement of the Fe with different transition metals.[20] In the current work, two systems were chosen to demonstrate the molecular doping strategy: the well-studied $(Fe_{1-x}Co_x)_3P$ spanning a range of precursor ratios,[19] and the $Fe_3(P_{1-x}Te_x)$ system to see if the molecular doping route could introduce tellurium to a metastable environment in several ratios.

As previously demonstrated, the molecular precursor $H_2Fe_3(CO)_9P^tBu$ (**I**, Figure 1) decomposes into phase pure, crystalline Fe_3P by MOCVD.[30] As a precursor with a nominal Co_3P

heavy element stoichiometry, $Co_3(CO)_9P^tBu$ (**II**, Figure 1) was selected to dope Co into the Fe_3P system.[31] As a precursor with a nominal Fe_3Te heavy element stoichiometry, $H_2Fe_3(CO)_9Te$ (**III**, Figure 1) was selected to dope Te into the Fe_3P system.[32] Individually, clusters **II** and **III** might not be expected to yield Co_3P and Fe_3Te materials upon decomposition as neither phase is known to be stable. However, as a mixture with compound **I** as the main constituent, decomposition favors the formation of the Fe_3P-type lattice.

In parallel with the target phase, each dopant cluster has a 3:1 metal to main group element ratio ensuring the metal or main group element is not lost or allowed to form inhomogeneities upon decomposition. Both of the dopant clusters are isostructural with **I** and have similar solubilities and volatilities, which allow for intimate mixing and uniform elemental distribution in the decomposition product. Cluster **III** is isoelectronic, while cluster **II** is a known exception to the cluster electron counting rules, being paramagnetic and possessing an extra electron as compared to the electron precise **I**.

Thin films of $(Fe_{1-x}Co_x)_3P$ ($0.09<x<0.22$) and $Fe_3(P_{1-x}Te_x)$ ($0.04<x<0.42$) were deposited by MOCVD co-decomposition of blend ranges $\mathbf{I}_{1-x}\mathbf{II}_x$ ($0.1<x<0.185$) and $\mathbf{I}_{1-x}\mathbf{III}_x$ ($0.05<x<0.49$), respectively. The phase purity and elemental composition of each film was confirmed via powder X-ray diffraction (PXRD), X-ray photoelectron spectroscopy (XPS), and inductively coupled plasma optical emission spectroscopy (ICP-OES). The changes in the magnetic properties of the doped Fe_3P thin films were studied via thermal gravimetric analysis (TGA) and magnetic property measurement system (MPMS).

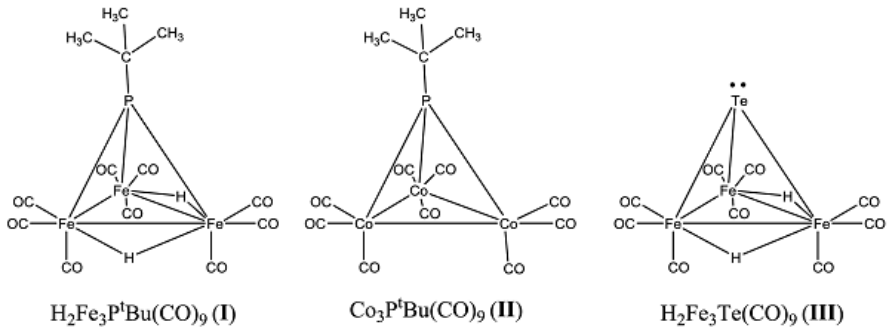

Figure 1: Metal Carbonyl Clusters used as Molecular Precursors

Experimental

Preparation of precursors

The precursors [$H_2Fe_3P^tBu(CO)_9$ (**I**)], [$Co_3P^tBu(CO)_9$ (**II**)] and [$H_2Fe_3Te(CO)_9$ (**III**)] were prepared according to previously reported procedures.[31–33] All precursors and thin films were stored under dry nitrogen to prevent oxidation. Tetrahydrofuran was dried (Pure Process Technology solvent purification system) and degassed (freeze, pump, thaw) before use. Homogeneous solid mixtures (blends) were made by weighing each single-source precursor under an inert atmosphere and combining in a Schlenk flask. The heterogeneous mixture was then dissolved in THF until homogeneous and the solvent was removed *in vacuo*. The molar ratios of the doped element to Fe_3P in the homogeneous blends and that of the subsequent thin films are shown in Table 1.

General Preparation of Precursor Blend

Organometallic precursors were combined in a glove box according to the amounts listed in Table 1. Degassed tetrahydrofuran (25 mL) was added and the solution stirred under an inert atmosphere until homogeneous. The solvent was removed in vacuo to yield an eggplant colored solid, which was transferred to the MOCVD for decomposition (*vide infra*) to yield the doped materials.

Table 1. Molar ratio of doped element to Fe_3P compared to that used in the precursor blend

Mass (g)		Blend Ratio (mol)		Thin Film Ratio (mol)	
I	**II**	**Co**	**Fe**	**Co**	**Fe**
0.18	0.02	1	9	1	10
0.21	0.03	1	7	1	7
0.26	0.06	1	4	1	3.5
I	**III**	**Te**	**P**	**Te**	**P**
0.19	0.01	1	9	1	25
0.14	0.06	1	4	1	4.5
0.11	0.11	1	1	1	1.4

Preparation of thin films

Quartz microscope slides were cut and mounted onto a stainless steel heating stage using silver paste. A modified version of the MOCVD apparatus used to manufacture thin films of phase-pure Fe_3P was used to deposit and anneal doped films (Figure 2).[30] Two improvements were the exchange of the borosilicate glass for quartz glass and a Kalrez O-ring at the joint for high temperatures. After the apparatus was loaded with the hot stage, a blend of precursors, and assembled in a glovebox, it was connected to a vacuum line. During the evacuation of the apparatus (8×10^{-6} Torr), the last two centimeters of Zone 2 were immersed in a liquid nitrogen bath. After Zone 1 was kept at 400 ºC for 1 hour, Zone 2 was brought to 125 ºC for 30 minutes. After the blend had disappeared and the substrate coated with the metallic film, Zone 1 was brought to 650 ºC for 24 hours for annealing.

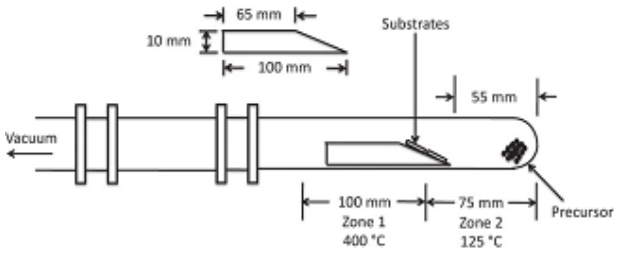

Figure 2. Schematic of quartz-walled MOCVD apparatus used to deposit doped thin films of Fe_3P.

Composition of the films

A Perkin Elmer ICP-OES with an internal yttrium standard was used for elemental analysis of the thin films to give percent composition of Fe, Co, P and Te. The films were digested in nitric acid in a sonication bath for 24 hours before analysis. Amounts of Fe, Co, P and Te were measured by spectral emission lines at 234.349, 228.616, 214.914 and 238.578 nm respectively. All of the elements were analyzed by axial viewing.

XPS measurements were made using a Physical Electronics PHI Quantera SXM instrument with a monochromatic aluminum Kα source operated at 40.7 W with a beam size of 200μm and a take-off angle of 45º. The films were sputtered with a 3 keV Ar^+ beam for 10 minutes before analyzing with a band pass of 26 eV to accurately determine Fe $2p_{3/2}$, P 2p and

Te $3d_5$ binding energies. The Co $2p_{3/2}$ binding energy falls within the iron auger lines and could not be measured quantitatively.

X-ray Diffraction Analysis

All of the X-ray diffraction (XRD) results were collected for the thin films deposited on the quartz slide with a Rigaku Ultima II vertical θ-θ powder diffractometer using Cu Kα radiation with Bragg-Brentano para-focusing optics. The lattice constants were obtained from the refinements by GSAS software.[34,35] The tetragonal space group $I\bar{4}$, lattice constants and atomic coordinates of the parent compound Fe_3P were used as the starting points for the refinements.[36] The final lattice constants are shown in Table 2.

Magnetic measurements and Curie temperature

Magnetic measurements were carried out using a Quantum Design Magnetic Property Measurement System (MPMS) on the materials peeled off of the quartz walls of the MOCVD apparatus and the quartz slides. Then, they were packed with TaegaSeal PTFE Tape in the measurement straw holder and the diamagnetic contribution due to the tape subtracted in all results.

Because the Curie temperatures of the materials are higher than the maximum temperature of MPMS, a Simultaneous DSC/TGA (SDT Q600) manufactured by TA instrument was employed. Taking advantage of the thermogravimetric analysis (TGA) function and intrinsic magnetic properties of the materials, five discs of neodymium magnets were placed on top of the instrument, reducing the measurable weight of the materials at room temperature. Upon ramping the temperature past the Curie temperature a sharp increment of the weight was observed due to the loss of magnetic attraction between the materials and magnets.[37] The Curie temperatures were determined by finding the maximum of the temperature derivative of measured weight.

Results & Discussion

Powders of the molecular precursors $Co_3(CO)_9P^tBu$ (**II**) or $H_2Fe_3(CO)_9Te$ (**III**) were combined with compound $H_2Fe_3(CO)_9P^tBu$ (**I**) by dissolving the combinations in THF until homogeneous then removing the solvent in vacuo to afford a homogeneous solid. The three different blends of **I** with **II** (9:1, 7:1 and 4.4:1) and **III** (21:1, 2.7:1 and 1:1) were prepared. These solid mixtures of single-source precursors were loaded into a quartz-walled MOCVD apparatus along with a stainless steel stage covered in quartz microscope slides. After the stage was preheated for one hour under vacuum, the precursors were heated and a shiny, metallic film deposited on both the walls of the MOCVD apparatus and the quartz slides on the hot stage. The region containing the stage was then annealed to produce crystalline thin films of $(Fe_{1-x}Co_x)_3P$ ($0.09<x<0.22$) and $Fe_3(P_{1-x}Te_x)$ ($0.04<x<0.42$).

The thin films were digested in trace metal grade nitric acid for ICP-OES analysis in order to determine the relative ratios of Fe, Co, Te and P. Although smaller amounts of the doped elements were found in the films than the amount in each blend, the values were all close to the expected value.

The Co-doped thin films were studied by XPS and the spectra for cobalt, iron and phosphorus are shown in Figure 3. The films were sputtered with Ar^+ for 2 minutes before measurements to remove the oxide layer that had formed on the surface. The spectrum for Fe consists of a single peak at 707 eV corresponding to the Fe $2p_{3/2}$ binding energy for metal phosphides.[38] The spectrum for phosphorus consists of two peaks at 129.5 and 130.5 eV corresponding to the phosphorus 2p and $2p_{1/2}$ binding energies. The spectrum for Co is hidden behind the Fe auger line, but in samples with larger amounts of a Co shoulder at 779 eV corresponding to the Co $2p_{3/2}$ binding energy can be observed. Because of this overlap, quantitative amounts of Co could not be determined via XPS. The binding energies found for each of the elements are in range of the zero oxidation state energies corresponding to metal phosphide materials.[38] A depth profile in a separate area was performed on the $(Fe_{1-x}Co_x)_3P$ thin film in such that the elemental composition was measured after 5 minute intervals of sputtering with Ar^+ (Figure 4). The percent composition of each element was uniform through the depth of the film and their relative ratios match the ICP-OES values of Fe_3P doped with Co. There was a small amount of oxygen with a binding energy of 531 eV corresponding to less than 2% of the

composition throughout the film. Sputtering was continued until the Fe and P dropped to zero and O increased to 100%, corresponding to the quartz substrate.

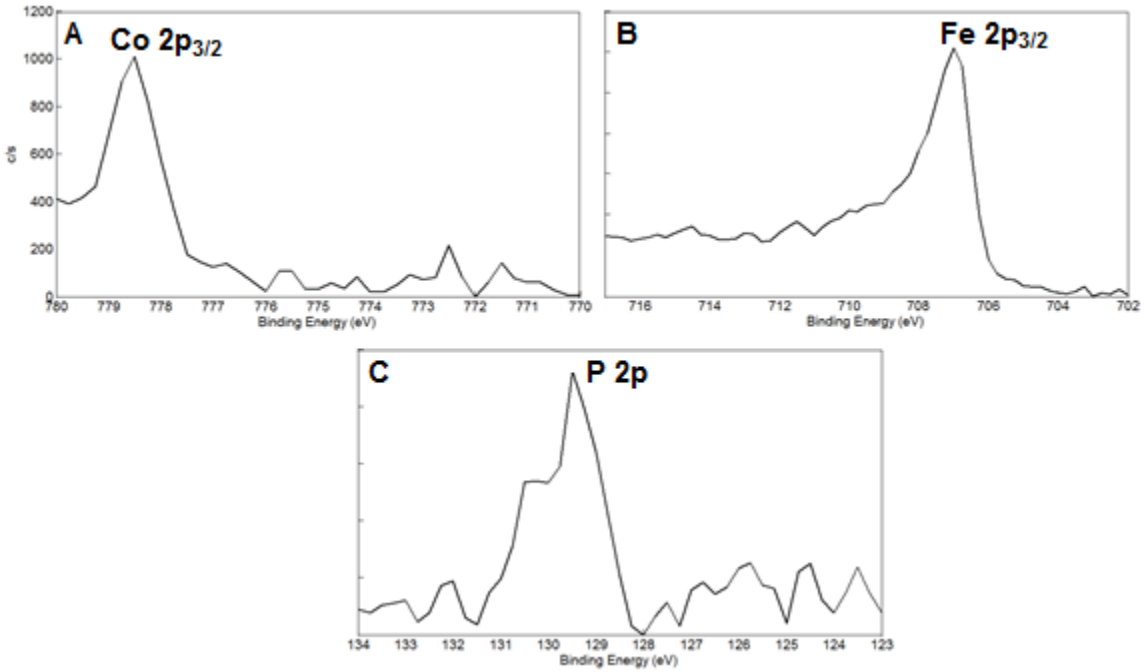

Figure 3. XPS spectrum for $(Fe_{1-x}Co_x)_3P$ (x = 0.09) showing low valent Fe (707 eV) and P (129 eV) (B and C respectively). Low valent Co (779 eV) is present on the shoulder of an Fe Auger line (A).

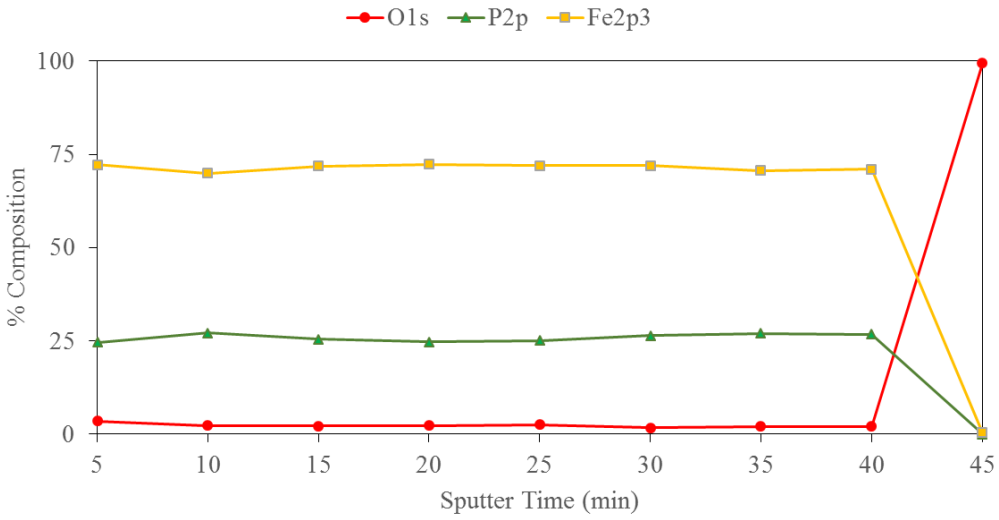

Figure 4. A representative XPS depth profile for $(Fe_{1-x}Co_x)_3P$ thin film showing homogeneity (x = 0.09).

The Te-doped thin films were studied by XPS and the spectra for Fe, Te, and P are shown in Figure 5. The films were sputtered with Ar^+ for 2 minutes before measurements to remove the oxide layer that had formed on the surface. The spectrum for Fe consists of a single peak at 707 eV corresponding to the Fe $2p_{3/2}$ binding energy for metal phosphides. The spectrum for Te consists of two peaks at 573 and 584 eV corresponding to the $3d_{5/2}$ and $3d_{3/2}$ binding energies. The spectrum for P consists of two peaks at 129.5 and 130.5 eV corresponding to the P 2p and $2p_{1/2}$ binding energies. The binding energies found for each of the elements are in range of the zero oxidation state binding energies corresponding to metal phosphide materials.[38] A depth profile in a separate area was performed on the $Fe_3(P_{1-x}Te_x)$ thin film in such that the elemental composition was measured after 5 minute intervals of sputtering with Ar^+ (Figure 6). The percent composition of each element was uniform through the depth of the film and their relative ratios match the ICP-OES values of Fe_3P doped with tellurium. There was a small amount of oxygen with a binding energy of 531 eV corresponding to less than 2% of the composition throughout the film. After the film was completely sputtered through the iron, tellurium and phosphorus amounts dropped to zero and the oxygen increased to 100%, corresponding to the quartz substrate.

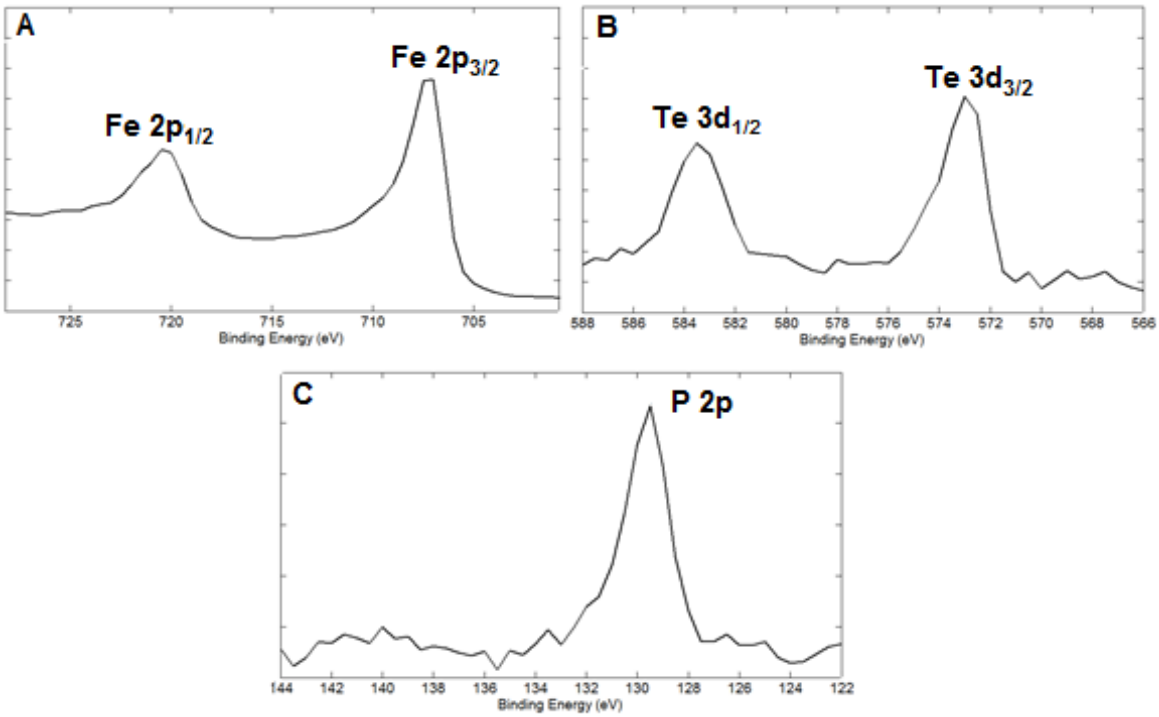

Figure 5. XPS spectrum for $Fe_3(P_x,Te_{1-x})$ (x = 0.18) showing low valent Iron (707 eV), Phosphorus (129 eV) and Tellurium (573 eV) (A, B and C respectively).

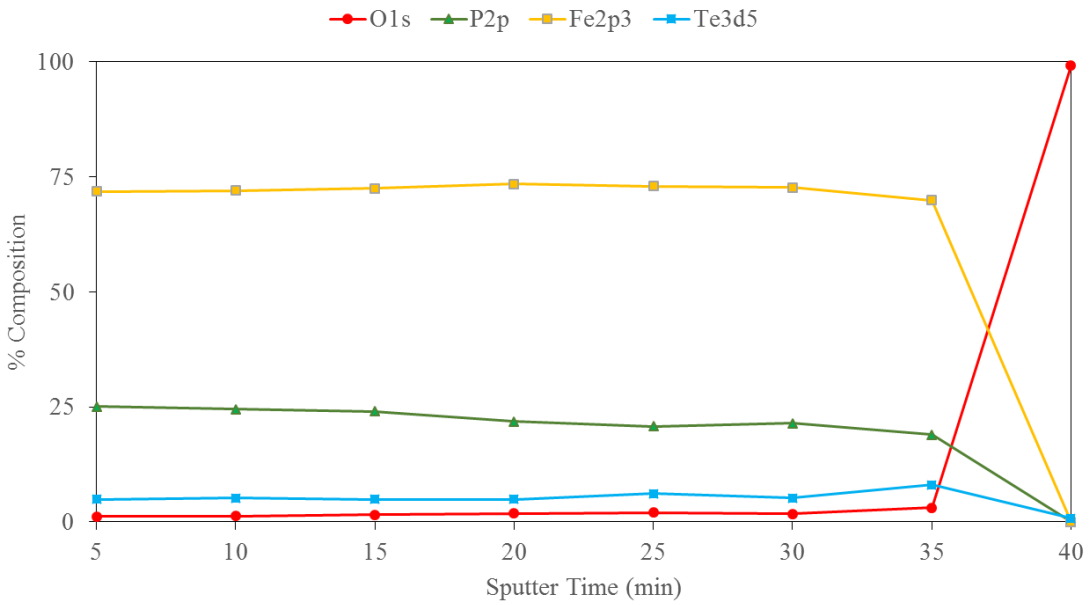

Figure 6. Representative XPS depth profile for $Fe_3(P_{1-x}Te_x)$ thin film showing homogeneity (x = 0.18).

X-Ray diffraction on as-deposited samples before annealing had poor signal to noise ratio, but were significantly improved by annealing at 650 ºC for 24 hours. The measured powder patterns for these thin films shown in Figure 7 match the Fe_3P pattern (space group $I\bar{4}$) with slight peak deviations that can be attributed to a change in unit cell constants arising from doping a third element into the Fe_3P parent compound. The lattice constant of the square plane (a=b) decreases while the c lattice constant remains unchanged in all cases. Furthermore, it was found that the lattice constants of square plane (a=b) decrease as the Co-dopant increases, which is in agreement with previously synthesized bulk Fe_3P doped with cobalt.[19] The final lattice constants are listed in Table 2.

In addition to differences in degree 2θ, there are deviations in peak intensities that track with the amount of the doped element. As the amount of doped-cobalt increases, the intensity of the peak at 35.9º decreases, which corresponds to the lattice plane (031). The lattice plane (031) runs through only metal atoms of the Fe_3P lattice, which explains why this peak does not change in the case of the Te-doped thin films. However, because the electron density of Co is close to

that of Fe, there is smaller intensity change. The lattice plane (240) running through the phosphorus and tellurium atoms of the Fe_3P lattice corresponds to $2\theta = 44.7^{o}$. Therefore, in the Te-doped films, the intensity at this angle increases as an incremental amount of P atoms are replaced with Te atoms. These changes in peak intensity can be attributed to the changes in atomic radius of the doped elements, smaller in the case of cobalt and larger in the case of tellurium.

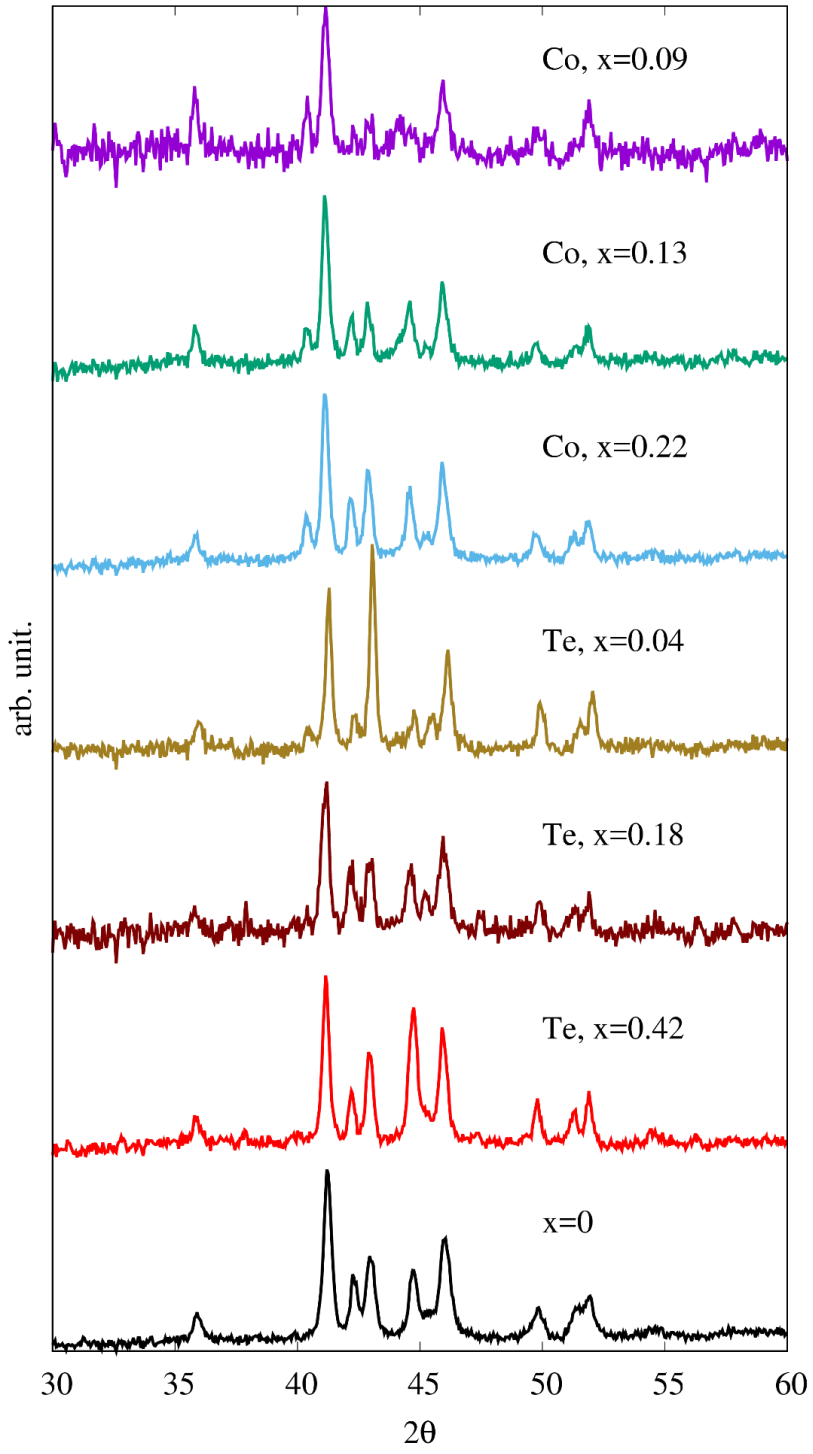

Figure 7. X-ray diffraction pattern of Fe_3P, $(Fe_{1-x}Co_x)_3P$ and $Fe_3(P_{1-x}Te_x)$ thin films after annealing.

Table 2. $(Fe_{1-x}Co_x)_3P$ and $Fe_3(P_{1-x}Te_x)$ compositions. The lattice constants were obtained from the refinement of space group $I\bar{4}$. The corresponding experimental results and analysis are shown.				
Sample	a(Å)	c(Å)	T_C (°C)	M_s**(μ_B)**
Pure Fe_3P (film)	9.1074	4.4602	412	5.1[39,40]
Co, x = 0.09	9.0917	4.4622	407	4.30337
Co, x = 0.13	9.0896	4.4625	405	3.76007
Co, x = 0.22	9.0761	4.4682	407	4.02293
Te, x = 0.04	9.0781	4.4549	413	4.32873
Te, x = 0.18	9.0849	4.4562	412	4.21718
Te, x = 0.42	9.0806	4.4591	413	4.43158

The experimental field-dependent magnetization data are shown in Figure 8. The magnetic hysteresis remains almost the same for all the cases. The saturation magnetization (M_s) was estimated from fitting of the experimental magnetization at high field using the law of approach-to-saturation (Equation 1) where K and K' are fitting parameters.[40]

$$M = M_s\left(1 - \frac{K}{H^2} - \frac{K'}{H^3}\right) \qquad (1)$$

The chemical compositions for the samples were obtained from ICP data in order to obtain the magnetization per formula unit (Fe_3P). The final results of the saturation moment for all six samples are listed in Table 2. They are found to be smaller than what was reported in pure bulk Fe_3P although no trend is found for the saturation magnetization changes as the dopant increases. Except (Co, x = 0.13), the saturation magnetic moments are close to each other while the Curie temperatures for the Te-doped Fe_3P is systematically larger than Co-doped Fe_3P. The difference of Curie temperature implies the interaction between magnetic atoms is lower in the Co-doped

Fe_3P than that of the Te-doped Fe_3P while the saturation magnetic moments remain close in all cases. The effect of substituting the transition metal with other metals in Fe_3P is already known to reduce the magnetic interaction and Curie temperature.[20] Te-doped Fe_3P is synthesized for the first time in the present work and the lack of effect of Te-doping on the Curie temperature indicates that Te elements must replace the atom positions occupied by P. Otherwise, the non-magnetic properties of Te would be expected to strongly reduce the magnetic interaction by replacing the magnetic elements such as Fe in our materials.

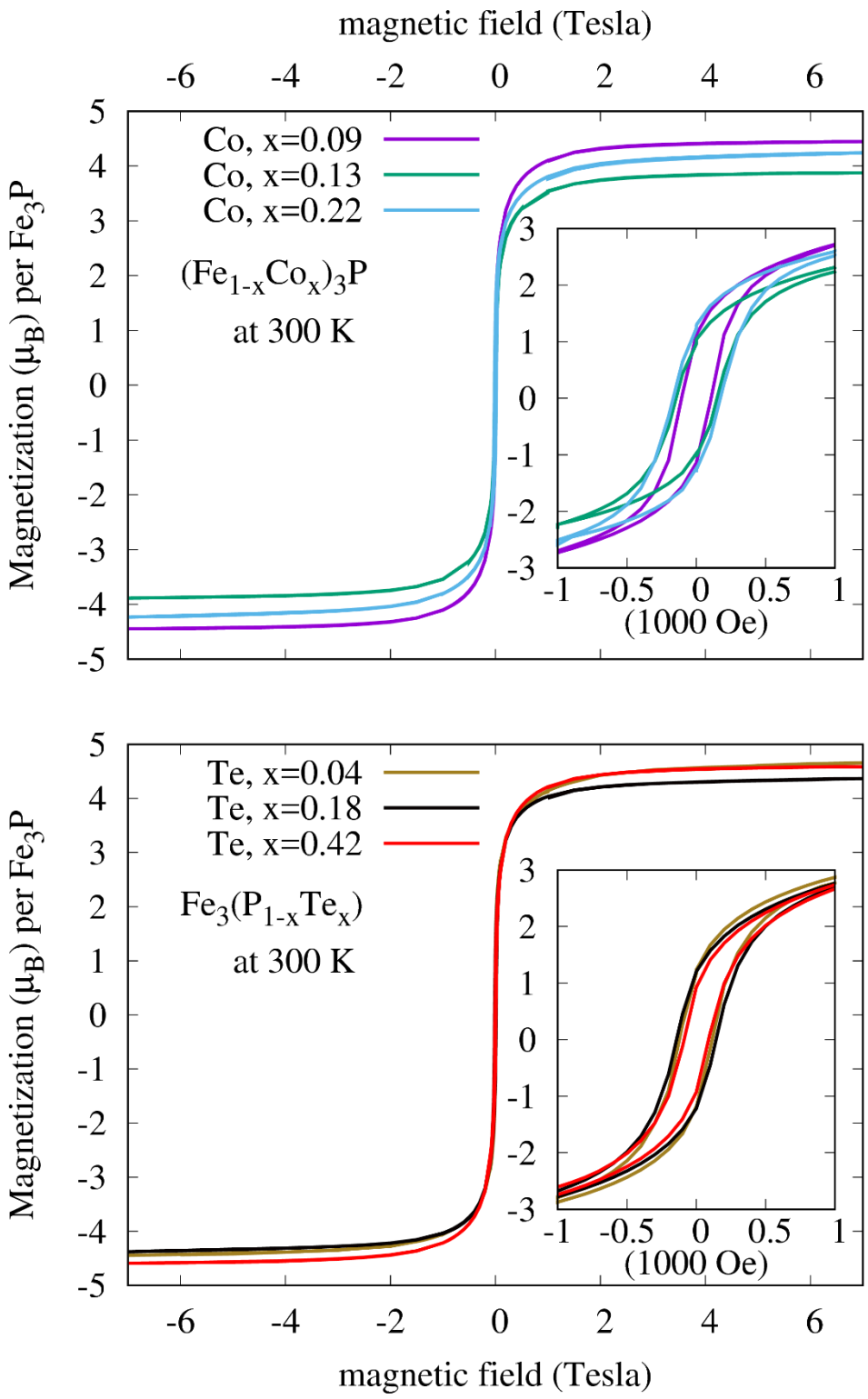

Figure 8. The field-dependent magnetization measurement were performed between -7 and 7 Tesla. The magnetic hysteresis in the small fields (< 0.1 Tesla) are shown in the inset.

Conclusions

Thin films of Fe_3P doped with Co and Te atoms has been achieved via the use of main group element metal carbonyl clusters as precursors for MOCVD. Combining organometallic single molecule clusters with respective predetermined stoichiometries as a solid solution and depositing the thin films on quartz afforded films with compositions that closely matched the heavy element stoichiometry of the solid blends. As expected, doping with elements of different sizes into the lattice caused changes in the unit cell parameters. While doping Te into the P site in the Fe_3P lattice had little to no effect on the magnetization of the material because the main group site has a negligible magnetic contribution, a decrease in the Curie temperature was observed by doping Co into Fe site in Fe_3P because the magnetic interaction between Fe sites are modified. The successful synthesis of thin films of ternary metal phosphides demonstrates the viability of the method and can be applied to other similar systems and possible quarternary phases.

Acknowledgements

This material is based upon work supported by the National Science Foundation Graduate Research Fellowship under Grant No. 1450681 and the National Science Foundation under Grant No. CHE-1411495. The authors also gratefully acknowledged for support of the Robert A. Welch Foundation (C-0976).

References:

(1) Zhuang, M.; Ou, X.; Dou, Y.; Zhang, L.; Zhang, Q.; Wu, R.; Ding, Y.; Shao, M.; Luo, Z. Polymer-Embedded Fabrication of Co_2P Nanoparticles Encapsulated in N,P-Doped Graphene for Hydrogen Generation. *Nano Lett.* **2016**.

(2) Li, D.; Arachchige, M. P.; Kulikowski, B.; Lawes, G.; Seda, T.; Brock, S. L. Control of Composition and Size in Discrete $Co_xFe_{2-x}P$ Nanoparticles: Consequences for Magnetic Properties. *Chem. Mater.* **2016**, *28* (11), 3920–3927.

(3) Tan, Y.; Wang, H.; Liu, P.; Cheng, C.; Zhu, F.; Hirata, A.; Chen, M. 3D Nanoporous Metal Phosphides toward High-Efficiency Electrochemical Hydrogen Production. *Adv. Mater.* **2016**, *28* (15), 2951–2955.

(4) Oyama, S. T. Novel Catalysts for Advanced Hydroprocessing: Transition Metal Phosphides. *J. Catal.* **2003**, *216* (1–2), 343–352.

(5) Layan Savithra, G. H.; Muthuswamy, E.; Bowker, R. H.; Carrillo, B. A.; Bussell, M. E.; Brock, S. L. Rational Design of Nickel Phosphide Hydrodesulfurization Catalysts: Controlling Particle Size and Preventing Sintering. *Chem. Mater.* **2013**, *25* (6), 825–833.

(6) Callejas, J. F.; McEnaney, J. M.; Read, C. G.; Crompton, J. C.; Biacchi, A. J.; Popczun, E. J.; Gordon, T. R.; Lewis, N. S.; Schaak, R. E. Electrocatalytic and Photocatalytic Hydrogen Production from Acidic and Neutral-pH Aqueous Solutions Using Iron Phosphide Nanoparticles. *ACS Nano* **2014**, *8* (11), 11101–11107.

(7) Zhang, H.; Ha, D.-H.; Hovden, R.; Kourkoutis, L. F.; Robinson, R. D. Controlled Synthesis of Uniform Cobalt Phosphide Hyperbranched Nanocrystals Using Tri- *N* -Octylphosphine Oxide as a Phosphorus Source. *Nano Lett.* **2011**, *11* (1), 188–197.

(8) Li, D.; Baydoun, H.; Verani, C. N.; Brock, S. L. Efficient Water Oxidation Using CoMnP Nanoparticles. *J. Am. Chem. Soc.* **2016**, *138* (12), 4006–4009.

(9) Bacmann, M.; Soubeyroux, J.-L.; Barrett, R.; Fruchart, D.; Zach, R.; Niziol, S.; Fruchart, R. Magnetoelastic Transition and Antiferro-Ferromagnetic Ordering in the System $MnFeP_{1-y}As_y$. *J. Magn. Magn. Mater.* **1994**, *134* (1), 59–67.

(10) Tobola, J.; Bacmann, M.; Fruchart, D.; Kaprzyk, S.; Koumina, A.; Niziol, S.; Soubeyroux, J.-L.; Wolfers, P.; Zach, R. Magnetism of Fe_2P Investigated by Neutron Experiments and Band Structure Calculations. *J. Magn. Magn. Mater.* **1996**, *157–158*, 708–710.

(11) Broddefalk, A.; James, P.; Liu, H.-P.; Kalska, B.; Andersson, Y.; Granberg, P.; Nordblad, P.; Häggström, L.; Eriksson, O. Structural and Magnetic Properties of $\{Fe_{1-x}Mn\}_3P$ ($x < 0.25$). *Phys. Rev. B* **2000**, *61* (1), 413–421.

(12) Silva, D. C. C.; Crosnier, O.; Ouvrard, G.; Greedan, J.; Safa-Sefat, A.; Nazar, L. F. Reversible Lithium Uptake by FeP_2. *Electrochem. Solid-State Lett.* **2003**, *6* (8), A162.

(13) Hall, J. W.; Membreno, N.; Wu, J.; Celio, H.; Jones, R. A.; Stevenson, K. J. Low-Temperature Synthesis of Amorphous FeP_2 and Its Use as Anodes for Li Ion Batteries. *J. Am. Chem. Soc.* **2012**, *134* (12), 5532–5535.

(14) Zhang, Z.; Lu, B.; Hao, J.; Yang, W.; Tang, J. FeP Nanoparticles Grown on Graphene Sheets as Highly Active Non-Precious-Metal Electrocatalysts for Hydrogen Evolution Reaction. *Chem. Commun.* **2014**, *50* (78), 11554–11557.

(15) Rundqvist, S.; Lundvik, L.; Hassler, E. Refinement of Ni_3P Structure. *Acta Chem. Scand.* **1962**, *16* (1), 242.

(16) Rundqvist, S. X-Ray Investigations of the Ternary System Fe-P-B. Some Features of the Systems Cr-P-B, Mn-P-B, Co-P-B and Ni-P-B. *Acta Chem. Scand.* **1962**, *16* (1), 1–19.

(17) Rundqvist, S. X-Ray Investigations of Mn_3P, Mn_2P, and Ni_2P. *Acta Chem. Scand.* **1962**, *16* (4), 992–998.

(18) Liu, H.; Andersson, Y.; James, P.; Satula, D.; Kalska, B.; Häggström, L.; Eriksson, O.; Broddefalk, A.; Nordblad, P. The Antiferromagnetism of $(Fe_{1-x}Mn_x)3P$, $x \geqslant 0.67$, Compounds. *J. Magn. Magn. Mater.* **2003**, *256* (1–3), 117–128.

(19) Liu, H.; James, P.; Broddefalk, A.; Andersson, Y.; Granberg, P.; Eriksson, O. Structural and Magnetic Properties of $(Fe_{1-x}Co_x)_3P$ Compounds: Experiment and Theory. *J. Magn. Magn. Mater.* **1998**, *189* (1), 69–82.

(20) Goto, M.; Tange, H.; Tokunaga, T.; Fujii, H.; Okamoto, T. Magnetic Properties of the $(Fe_{1-x}M_x)_3P$ Compounds. *Jpn. J. Appl. Phys.* **1977**, *16* (12), 2175.

(21) Kelly, A. T.; Rusakova, I.; Ould-Ely, T.; Hofmann, C.; Lüttge, A.; Whitmire, K. H. Iron Phosphide Nanostructures Produced from a Single-Source Organometallic Precursor: Nanorods, Bundles, Crosses, and Spherulites. *Nano Lett.* **2007**, *7* (9), 2920–2925.

(22) Colson, A. C.; Whitmire, K. H. Synthesis of $Fe_{2-x}Mn_xP$ Nanoparticles from Single-Source Molecular Precursors. *Chem. Mater.* **2011**, *23* (16), 3731–3739.

(23) Bauer, S.; Hunger, C.; Bodensteiner, M.; Ojo, W.-S.; Cros-Gagneux, A.; Chaudret, B.; Nayral, C.; Delpech, F.; Scheer, M. Transition-Metal Complexes Containing Parent Phosphine or Phosphinyl

Ligands and Their Use as Precursors for Phosphide Nanoparticles. *Inorg. Chem.* **2014**, *53* (21), 11438–11446.

(24) Hunger, C.; Ojo, W.-S.; Bauer, S.; Xu, S.; Zabel, M.; Chaudret, B.; Lacroix, L.-M.; Scheer, M.; Nayral, C.; Delpech, F. Stoichiometry-Controlled FeP Nanoparticles Synthesized from a Single Source Precursor. *Chem. Commun.* **2013**, *49* (100), 11788–11790.

(25) Colson, A. C.; Chen, C.-W.; Morosan, E.; Whitmire, K. H. Synthesis of Phase-Pure Ferromagnetic Fe_3P Films from Single-Source Molecular Precursors. *Adv. Funct. Mater.* **2012**, *22* (9), 1850–1855.

(26) Schmitt, A. L.; Higgins, J. M.; Jin, S. Chemical Synthesis and Magnetotransport of Magnetic Semiconducting $Fe_{1-x}Co_xSi$ Alloy Nanowires. *Nano Lett.* **2008**, *8* (3), 810–815.

(27) Higgins, J. M.; Carmichael, P.; Schmitt, A. L.; Lee, S.; Degrave, J. P.; Jin, S. Mechanistic Investigation of the Growth of $Fe_{1-x}Co_xSi$ ($0 \le X \le 1$) and $Fe_5(Si_{1-y}Ge_y)_3$ ($0 \le Y \le 0.33$) Ternary Alloy Nanowires. *ACS Nano* **2011**, *5* (4), 3268–3277.

(28) Pan, Y.; Liu, Y.; Lin, Y.; Liu, C. Metal Doping Effect of the M–Co_2P/Nitrogen-Doped Carbon Nanotubes (M = Fe, Ni, Cu) Hydrogen Evolution Hybrid Catalysts. *ACS Appl. Mater. Interfaces* **2016**, *8* (22), 13890–13901.

(29) Delczeg-Czirjak, E. K.; Delczeg, L.; Punkkinen, M. P. J.; Johansson, B.; Eriksson, O.; Vitos, L. *Ab Initio* Study of Structural and Magnetic Properties of Si-Doped Fe_2P. *Phys. Rev. B* **2010**, *82* (8), 85103.

(30) Colson, A. C.; Chen, C.-W.; Morosan, E.; Whitmire, K. H. Synthesis of Phase-Pure Ferromagnetic Fe3P Films from Single-Source Molecular Precursors. *Adv. Funct. Mater.* **2012**, *22* (9), 1850–1855.

(31) Marko, L.; Markó, B. Paramagnetic Phosphido Cobalt Carbonyl Clusters. *Inorganica Chim. Acta* **1975**, *14*, L39.

(32) Bachman, R. E.; Whitmire, K. H.; Hal, J. van. Effect of Charge on Structure: Stepwise Protonation of $[EFe_3(CO)_9]^{2-}$ (E = Se, Te) and Isolation of a Novel Mixed-Metal Cluster $[TeFe_3(CO)_9(\mu\text{-CuCl})]^{2-}$. *Organometallics* **1995**, *14* (4), 1792–1801.

(33) Huttner, G.; Schneider, J.; Mohr, G.; Seyerl, J. V. R-P-Verbrückte Eien-Cluster-Hydride. *J. Organomet. Chem.* **1980**, *191* (1), 161–169.

(34) Larson, A. C.; Dreele, R. B. V. *Los Alamos Natl. Lab. Rep. LAUR* **1994**, 86–748.

(35) Toby, B. H. It EXPGUI, a Graphical User Interface for It GSAS. *J. Appl. Crystallogr.* **2001**, *34* (2), 210–213.

(36) Spriggs, P. H. An Investigation of the Variation of Lattice Parameters with Composition along the Tie-Line Ni_3P-Fe_3P. *Philos. Mag.* **1970**, *21* (173), 897–901.

(37) Standard Practice for Calibration of Temperature Scale for Thermogravimetry. *ASTM Int. West Conshohocken* **2000**.

(38) Blanchard, P. E. R.; Grosvenor, A. P.; Cavell, R. G.; Mar, A. X-Ray Photoelectron and Absorption Spectroscopy of Metal-Rich Phosphides M_2P and M_3P (M = Cr−Ni). *Chem. Mater.* **2008**, *20* (22), 7081–7088.

(39) Lisher, E. J.; Wilkinson, C.; Ericsson, T.; Haggstrom, L.; Lundgren, L.; Wappling, R. Studies of the Magnetic Structure of Fe_3P. *J. Phys. C Solid State Phys.* **1974**, *7* (7), 1344.

(40) Meyer, A. J. P.; Cadeville, M. C. Magnetic Properties of Iron-Phosphorus Compounds. *J. Phys. Soc. Jpn.* **1962**, *17* (B1), 223–225.

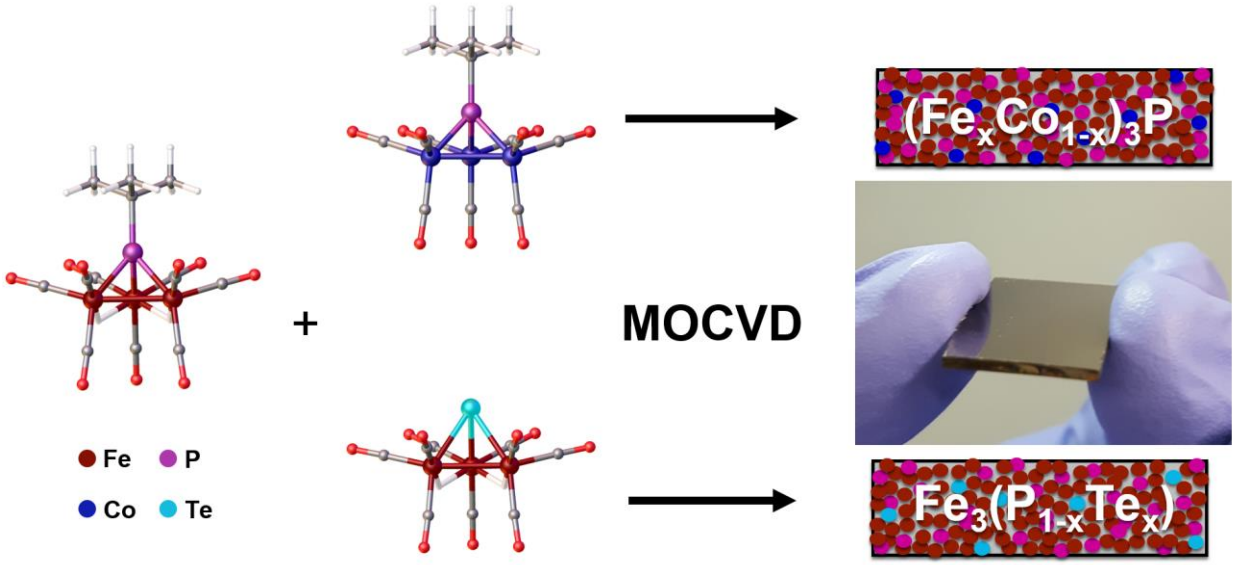
Fe
P
Co
Te
+
MOCVD
$(Fe_xCo_{1-x})_3P$
$Fe_3(P_{1-x}Te_x)$